Impacts of PLL on the DFIG-based WTG's Electromechanical Response Under Transient Conditions: Analysis and Modeling

Dongliang Zhang, *Student Member, IEEE*, Yajing Wang, Jiabing Hu, *Senior Member, IEEE*, Shicong Ma, *Member, IEEE*, Qing He, and Qiang Guo

***Abstract*—Increased penetration of wind energy in the electric grid has necessitated studying the impact of wind integration on the transient stability of the power system, with urgency to develop appropriate electromechanical models of the wind turbine generator (WTG). The representation and control of the WTG's electric signals are typically in a rotational dq coordinate system whose reference angle is provided by a phase-locked-loop (PLL). The PLL is commonly considered as a measurement device and is often absent in existing WTG electromechanical models. This paper studies the impact of PLL on the DFIG-based WTG electromechanical response by theoretical and simulation analyses. The dynamics of the PLL are found to greatly influence the WTG electromechanical response, suggesting that PLL should be regarded as an indispensable control loop rather than a measurement device, and its impact should be modeled when establishing the WTG electromechanical model.**

***Index Terms*—DFIG-based WTG, electromechanical model, phase-locked-loop (PLL), transient stability.**

NOMENCLATURE

$i_{\mathrm{d}}^{\mathrm{p}}, i_{\mathrm{q}}^{\mathrm{p}}$	d-axis and q-axis current components represented in the rotational dq coordinate system established by the PLL.
$i_{\mathrm{d}}, i_{\mathrm{q}}$	d-axis and q-axis current components represented in the rotational dq coordinate system established directly by the terminal voltage.
$\boldsymbol{V_t}, \boldsymbol{I}$	Rotating vectors of the terminal voltage and the WTG injecting current.
$\omega_{V_{\mathrm{t}}}, \omega_{\mathrm{pll}}$	Rotating speeds of the terminal voltage vector and the d-axis of the PLL dq coordinate system.
$R_{\mathrm{s}}, L_{\mathrm{s}}, L_{\mathrm{m}}$	Stator resistance, stator self-inductance, and mutual inductance of the DFIG generator.
$\boldsymbol{\Psi_{\mathrm{s}}}$	Stator flux linkage vector of the DFIG generator.
$V_{\mathrm{td}}^{\mathrm{p}}, V_{\mathrm{tq}}^{\mathrm{p}}$	d-axis and q-axis components of the terminal voltage in the rotational dq coordinate system establshed by the PLL.
$i_{\mathrm{rd}}^{\mathrm{p}}, i_{\mathrm{rq}}^{\mathrm{p}}$	d-axis and q-axis components of the magnetizing current of the rotor-side converter in the rotational dq coordinate system established by the PLL.
$i_{\mathrm{sd}}^{\mathrm{p}}, i_{\mathrm{sq}}^{\mathrm{p}}$	d-axis and q-axis components of the DFIG stator current in the rotational dq coordinate system established by the PLL.
$i_{\mathrm{r\_max}}$	Current capacity of the rotor-side converter.

Manuscript received September 25, 2015; revised January 12, 2016; accepted April 6, 2016. Date of publication June 30, 2016; date of current version May 3, 2016. This work was supported by Science and Technology Program of State Grid Corporation of China under Grant XT71-14-051.

D. Zhang and J. Hu (corresponding author, e-mail: j.hu@hust.edu.cn) are with State Key Laboratory of Advanced Electromagnetic Engineering and Technology, and Huazhong University of Science and Technology, Wuhan 430074, China.

Y. Wang is with Ningbo Electric Power Design Institute Co. Ltd., Ningbo 315000, China.

S. Ma, Q. He, and Q. Guo are with China Electric Power Research Institute, Beijing 100192, China.

DOI: 10.17775/CSEEJPES.2016.00019

I. INTRODUCTION

WIND energy is being promoted today globally to reduce the consumption of fossil fuels and the emission of greenhouse gases [1]. Wind power typically employs a converter-based generator of which the transient dynamics are different from traditional synchronous generators, thus requiring that its impact on power system stability be assessed properly. Currently, this assessment is typically conducted using time-domain simulations, which require appropriate modeling of the electromechanical response of the wind turbine generator (WTG) under transient conditions.

The various WTG models [2]–[18] are generally divided into 1) a full-order model and 2) a reduced-order model. The full-order model keeps all the control loops and can provide the most accurate response. However, the high order of the full-order model limits the speed and the scale of the simulation. In addition, the full-order model is not only always provided by the WTG manufacturers, and also is protected under a non-disclosure agreement. Consequently, it is difficult for the public to get access to these models.

The reduced-order model increases the simulation speed and the simulation scale by ignoring or simplifying some control loops, while still satisfying the accuracy requirements of specific study purposes. There are various reduced-order models for various study purposes, such as for power quality [2], voltage dip ride-through [3], short-circuit calculation [4], DC-link voltage stability [5], singularity-induced instability [6], subsynchronous oscillation [7], and transient stability [8]–[18]. Among these, the electromechanical reduced-order model for

transient stability has received extensive attention. Several working groups, such as the Western Electricity Coordinating Council (WECC) Renewable Energy Modeling Task Force (REMTF), and the International Electrotechnical Commission (IET) Technical Committee (TC) 88, have all been established for the purpose of studying this model, with many publications related to the generic electromechanical WTG models [15]–[18].

Existing electromechanical models treat the PLL as a typical measurement device instead of an indispensable control loop of the WTG. Much like other measurement devices for voltage, current, and rotating speed, the dynamics of the PLL in these electromechanical models have received little study. The WTG terminal voltage is used to directly establish the rotational dq coordinate system.

This paper studies the impact of the PLL on the transient electromechanical response of the DFIG-based WTG. Section II presents the theoretical analysis. Section III presents the simulation analysis. This study shows the considerate influence that the PLL has on the WTG electromechanical responses and the need to incorporate this impact into the WTG model for transient stability studies.

II. Theoretical Analysis

A. Role of the PLL in the DFIG-based WTG

As Fig. 1 shows, the electric signals of the DFIG-based WTG are represented and controlled in a rotational dq coordinate system while those of the external grid are in a static abc coordinate system. As a result, the electric signals are required to change their coordinate systems during the exchange between the WTG and the external grid. The successful operation of the WTG relies on synchronization of the rotational dq coordinate system with the rotational terminal voltage vector. The terminal voltage vector can be synthesized by its a-axis, b-axis, and c-axis components in the static abc coordinate system. Fig. 2 demonstrates the results of the synchronization.

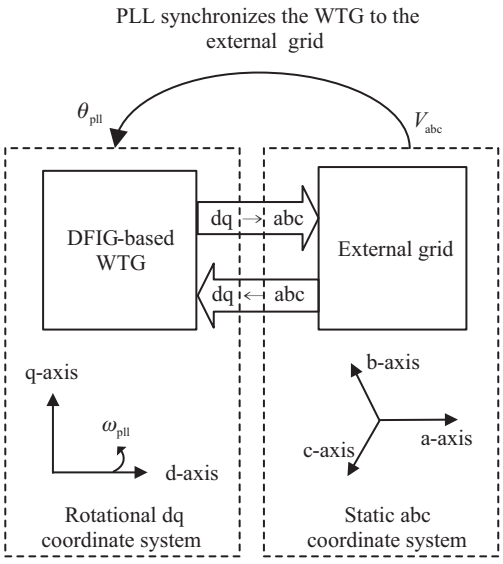

Fig. 1. Role of the PLL in a grid-connected DFIG-based WTG.

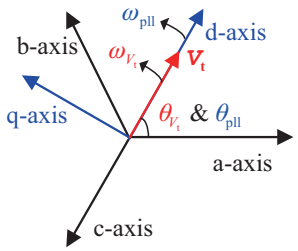

Fig. 2. Synchronization of the rotational dq coordinate system and the rotational terminal voltage vector.

The d-axis of the rotational dq coordinate system always coincides with the rotational vector of the terminal voltage. In other words, to achieve the synchronization, the phase of the rotational d-axis of the dq coordinate system should always be equal to that of the rotational vector of the terminal voltage. Typically, a PLL is employed to generate the d-axis phase reference that is always equal to the phase of the terminal voltage vector, i.e.,

$$\theta_{\mathrm{pll}} = \theta_{V_{\mathrm{t}}} \tag{1}$$

The resulting WTG dq coordinate system based on the output phase of the PLL will synchronize with the terminal voltage vector.

Fig. 3 shows the framework of the PLLs employed by the WTGs [19]. Here, the phase detector transforms the coordinate system of the terminal voltage from the static abc coordinate system of the external grid to the rotational dq coordinate system of the PLL. The d-axis and q-axis components of the terminal voltage, V_{td} and V_{tq}, are then further processed by the monotonous transfer module to form an error signal, which is monotonous to the phase difference between the d-axis of the PLL's rotating dq coordinate system and the rotational terminal voltage vector. Then the phase error regulator will regulate the error signal and generate the rotating speed or frequency of the dq coordinate system, which will be integrated to obtain the phase of the d-axis θ_{pll}. The θ_{pll} will be used to establish the rotational dq coordinate systems of the PLL and the WTG.

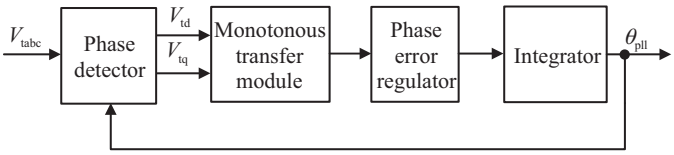

Fig. 3. Schematic of the PLLs employed by the WTGs.

B. Impacts of the PLL on the Electromechanical Response of the DFIG-based WTG

The electromechanical model of the DFIG-based WTG typically does not factor in the current control loops since their bandwidth is over 100 Hz, which is much higher than the bandwidth range (below 15 Hz) required in the electromechanical analysis [20]. As a result, compared to the bidirectional exchange shown in Fig. 1, the exchange of the electric signal between the WTG and the grid becomes unidirectional, which

is illustrated in Fig. 4. Only the WTG output current needs to be transformed from the dq coordinate system to the abc coordinate system. The transformation can be expressed as

$$\begin{bmatrix} i_{\mathrm{a}} \\ i_{\mathrm{b}} \\ i_{\mathrm{c}} \end{bmatrix} = \begin{bmatrix} \cos\theta_{\mathrm{pll}} & -\sin\theta_{\mathrm{pll}} \\ \cos(\theta_{\mathrm{pll}} - \frac{2\pi}{3}) & -\sin(\theta_{\mathrm{pll}} - \frac{2\pi}{3}) \\ \cos(\theta_{\mathrm{pll}} + \frac{2\pi}{3}) & -\sin(\theta_{\mathrm{pll}} + \frac{2\pi}{3}) \end{bmatrix} \begin{bmatrix} i_{\mathrm{d}}^{\mathrm{p}} \\ i_{\mathrm{q}}^{\mathrm{p}} \end{bmatrix} \quad (2)$$

where θ_{pll} is the output phase of the PLL.

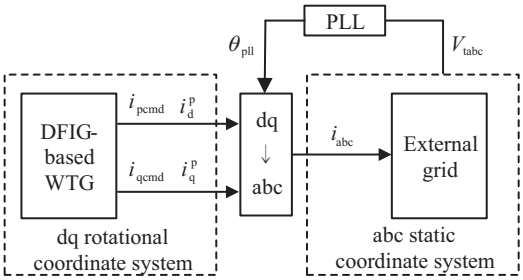

Fig. 4. Unidirectional electric signal flow between the WTG electromechanical model and the external grid.

Another result of not factoring in the current control loops is that the d-axis component of the WTG current will always equal the active current commander, and the q-axis component will always equal the reactive current commander.

$$i_{\mathrm{d}}^{\mathrm{p}} = i_{\mathrm{pcmd}} \quad (3)$$

$$i_{\mathrm{q}}^{\mathrm{p}} = i_{\mathrm{qcmd}} \quad (4)$$

Under normal conditions, the rotating d-axis of the PLL dq coordinate system will lock to the rotating vector of the terminal voltage, as shown in Fig. 2. The relationships between active current component i_{p}, reactive current component i_{q}, d-axis current component $i_{\mathrm{d}}^{\mathrm{p}}$, and q-axis current component $i_{\mathrm{q}}^{\mathrm{p}}$ of the WTG output current are demonstrated in Fig. 5. As shown, the WTG active current is equal to the d-axis component current and the reactive current component is equal to the q-axis component current.

$$i_{\mathrm{p}} = i_{\mathrm{d}}^{\mathrm{p}} \quad (5)$$

$$i_{\mathrm{q}} = i_{\mathrm{q}}^{\mathrm{p}} \quad (6)$$

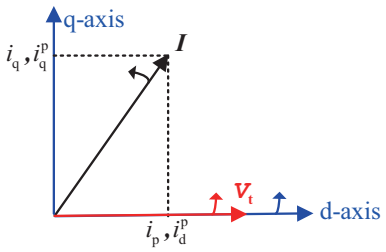

Fig. 5. Current and voltage phasor diagram when the PLL dq coordinate system locks to the terminal voltage vector.

Substituting (3)–(4) into (5)–(6) gives

$$i_{\mathrm{p}} = i_{\mathrm{pcmd}} \quad (7)$$

$$i_{\mathrm{q}} = i_{\mathrm{qcmd}} \quad (8)$$

Equations (7)–(8) indicate that under normal conditions the active and reactive currents of the DFIG-based WTG are determined exclusively by the respective active and reactive current commanders.

However, large disturbances such as the occurrence of a short-circuit fault and the disconnection of a faulted line may cause a sharp jump in the terminal voltage rotating vector phase. This phase jump is considered a step disturbance to the PLL, which causes the PLL to lose synchronization with the terminal voltage vector. Before the PLL retrieves the synchronization, there will be a phase difference between the rotating d-axis and rotating voltage vector, which is defined as

$$\Delta\theta = \theta_{V_{\mathrm{t}}} - \theta_{\mathrm{pll}} \quad (9)$$

and demonstrated in Fig. 6. From Fig. 6, the changed relationships of the active current component i_{p}, reactive current component i_{q}, d-axis current component $i_{\mathrm{d}}^{\mathrm{p}}$, and q-axis current component $i_{\mathrm{q}}^{\mathrm{p}}$ of the WTG output current are obtained

$$i_{\mathrm{p}} = i_{\mathrm{d}}^{\mathrm{p}}\cos\Delta\theta + i_{\mathrm{q}}^{\mathrm{p}}\sin\Delta\theta \quad (10)$$

$$i_{\mathrm{q}} = -i_{\mathrm{d}}^{\mathrm{p}}\sin\Delta\theta + i_{\mathrm{q}}^{\mathrm{p}}\cos\Delta\theta \quad (11)$$

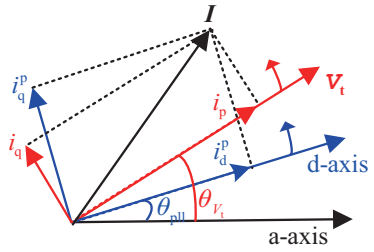

Fig. 6. Current and voltage phasor diagram when the PLL dq coordinate system does not lock to the terminal voltage vector.

Substituting (3)–(4) into (10)–(11) gives

$$i_{\mathrm{p}} = i_{\mathrm{pcmd}}\cos\Delta\theta + i_{\mathrm{qcmd}}\sin\Delta\theta \quad (12)$$

$$i_{\mathrm{q}} = -i_{\mathrm{pcmd}}\sin\Delta\theta + i_{\mathrm{qcmd}}\cos\Delta\theta \quad (13)$$

Equations (12)–(13) suggest that when the PLL loses synchronization after being subjected to a large disturbance in the external grid, the active and reactive currents of the WTG are determined by a combination of the active current commander, the reactive current commander and the phase difference instead of the respective active or reactive current commander alone which is the case when the PLL keeps the synchronization with the terminal voltage vector.

C. Impacts of Neglecting the PLL on the Electromechanical Response of the DFIG-based WTG

The common practice of the existing DFIG-based WTG electromechanical models is to neglect the PLL, as shown in Fig. 7. In this instance, the transformation of the WTG current from the rotational dq coordination system into the static abc coordinate system will not depend on the output phase of the PLL; rather, it will directly rely on the three phase terminal voltages. The changed transformation can then be expressed as

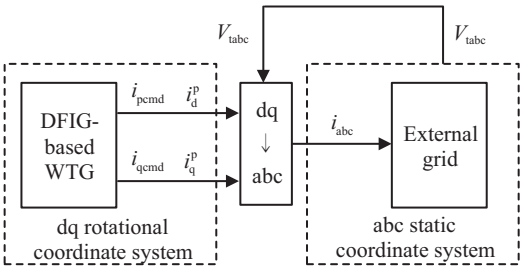

Fig. 7. Neglect of the PLL in the existing DFIG-based WTG electromechanical model.

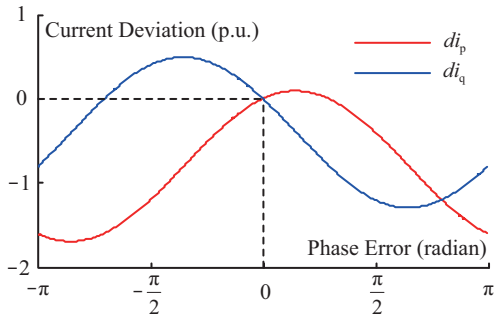

Fig. 8. WTG active and reactive current deviations resulted form the phase error between the PLL and the terminal voltage.

$$\begin{bmatrix} i_a \\ i_b \\ i_c \end{bmatrix} = \begin{bmatrix} \cos\theta_{V_t} & -\sin\theta_{V_t} \\ \sin\theta_{V_t} & \cos\theta_{V_t} \end{bmatrix} \begin{bmatrix} 1 & 0 \\ -\frac{1}{2} & \frac{\sqrt{3}}{2} \\ -\frac{1}{2} & -\frac{\sqrt{3}}{2} \end{bmatrix} \begin{bmatrix} i_d^p \\ i_q^p \end{bmatrix} \tag{14}$$

where θ_{V_t} is the phase of the rotating vector of the terminal voltage, and

$$\begin{bmatrix} \cos\theta_{V_t} \\ \sin\theta_{V_t} \end{bmatrix} = \frac{2}{3} \begin{bmatrix} 1 & -\frac{1}{2} & -\frac{1}{2} \\ 0 & \frac{\sqrt{3}}{2} & -\frac{\sqrt{3}}{2} \end{bmatrix} \begin{bmatrix} v_{ta} \\ v_{tb} \\ v_{tc} \end{bmatrix} \tag{15}$$

where v_{ta} v_{tb} v_{tc} are the three phase terminal voltages of the external grid in p.u.

The relationships between the active current component i_p, reactive current component i_q, d-axis current component i_d^p, and q-axis current component i_q^p of the WTG output current are

$$i_p = i_{pcmd} \tag{16}$$

$$i_q = i_{qcmd} \tag{17}$$

under normal and fault conditions.

According to (7)–(8) and (16)–(17), not considering the PLL will result in a same current response of the WTG under normal conditions. However, under fault conditions, according to (12)–(13) and (16)–(17), ignoring the PLL will lead to a deviated current response of the WTG. The deviations are represented by

$$\begin{aligned} di_p &= i_{p\_withpll} - i_{p\_withoutpll} \\ &= i_{pcmd}\cos\Delta\theta + i_{qcmd}\sin\Delta\theta - i_{pcmd} \end{aligned} \tag{18}$$

$$\begin{aligned} di_q &= i_{q\_withpll} - i_{q\_withoutpll} \\ &= -i_{pcmd}\sin\Delta\theta + i_{qcmd}\cos\Delta\theta - i_{qcmd} \end{aligned} \tag{19}$$

Fig. 8 shows the resulting active and reactive current deviations when the phase difference ranges from $-\pi$ to π. The active current commander is set to 0.8 p.u. and the reactive current commander is 0.5 p.u. Fig. 8 indicates that the neglect of PLL could cause significant deviations in the WTG currents.

D. Bandwidth of the PLL

The bandwidth of the PLL employed by the WTG involves a trade-off between two factors, the time response and the filtering performance. A larger bandwidth will result in a faster time response, which means that the PLL will need shorter time to resynchronize to the terminal voltage. A larger bandwidth also means a deteriorated filtering performance of the distortions of the grid voltage such as the harmonics and the asymmetrical elements [21]. As a result, the typical range of the PLL bandwidth is 8 to 25 Hz [22], and the control systems of the models for power system time-domain simulation are typically required to be valid up to 10 to 15 Hz [20]. The typical bandwidth of the PLL is in or close to the valid range of control systems. Therefore, the aforementioned impacts of the PLL on the WTG are in or close to the electromechanical time scale, and should be modeled when developing a WTG electromechanical model.

III. Simulation Analysis

A. Proposed DFIG-based WTG Electromechanical Model

This section describes a DFIG-based WTG reduced-order eletromechanical model that models the impacts of the PLL by incorporating the PLL in the model. The overall structure of the model is shown in Fig. 9. The proposed reduced-order electromechanical model is essentially a controlled-current-source consisting of two sub-controlled current sources representing the two interfaces from which the DFIG-based WTG injects current into the external grid, DFIG stator and grid-side converter.

1) Mechanical Model

The mechanical model, shown in Fig. 10, presents the control loops and the elements that affect the electromechanical-time-scale dynamics of the electric torque commander T_e. The control loops of the mechanical model are designed to maximize the electric power output under normal conditions, which is known as the maximum power point tracking (MPPT). Under fault conditions, the control loops and their parameter settings remain the same as the normal conditions though the MPPT has become technologically impossible.

The implementation of the MPPT is achieved by adjusting the rotating speed reference ω_r^* based on the electric power output P_e. The speed error between the speed reference and actual speed will be sent to the pitch controller and the electric torque controller. The pitch controller adjusts the speed error by adjusting the mechanical power input of the rotating mass through changing the pitch angle of the blades β. The electric torque controller adjusts the speed error ω_{err} by adjusting

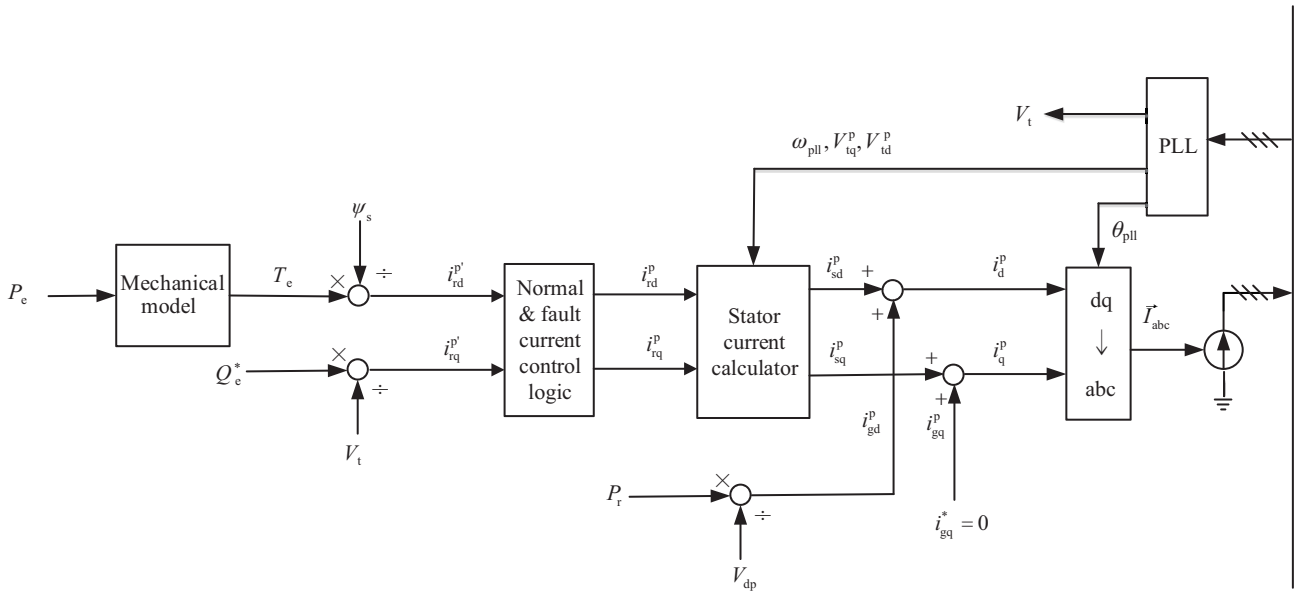

Fig. 9. Overall structure of the proposed DFIG-based WTG reduced-order eletromechanical model.

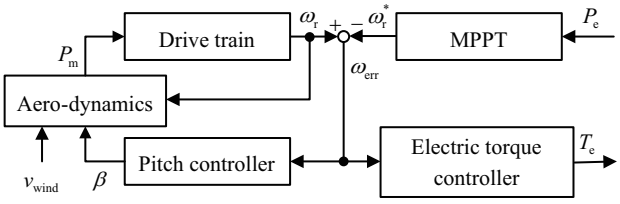

Fig. 10. Structure of the mechanical model.

the electric power output and changing the electric torque commander T_{e}. The rotating masses of the WTG are factored in the drive train, which is a two-mass model, representing two groups of the rotating masses, i.e., the turbine and the generator. The aerodynamics are simplified to

$$P_{\mathrm{m}} = \frac{\rho}{2} A_{\mathrm{r}} v_{\mathrm{wind}}^3 C_{\mathrm{p}}(\lambda, \beta) \tag{20}$$

where ρ is the air density, A_{r} is the sweeping area of the blades, v_{wind} is the wind speed, C_{p} is the power coefficient, λ is the ratio of the turbine blade tip speed and the wind speed, and β is the pitch angle. The details of the simplified aerodynamic can be found in [13].

2) Normal/Fault Current Control Logic

The electric commander T_{e} generated by the mechanical model is transformed to the WTG active current commander or the d-axis rotor current commander $i_{\mathrm{rd}}^{\mathrm{p}'}$, which, along with the reactive or q-axis current commander $i_{\mathrm{rq}}^{\mathrm{p}'}$ generated by the outer Q/V control loop, is then sent to the normal/fault current control logic to form the eventual d-axis and q-axis rotor magnetizing currents $i_{\mathrm{rd}}^{\mathrm{p}}$ and $i_{\mathrm{rq}}^{\mathrm{p}}$. Fig. 11 demonstrates the workflow of the logic.

Under normal conditions, the logic ensures that the eventual apparent magnetizing current does not exceed the current capacity of the rotor-side converter $i_{\mathrm{r\_max}}$. In addition, the logic endows the d-axis rotor current commander, i.e., the WTG active current commander with the priority in the allocation

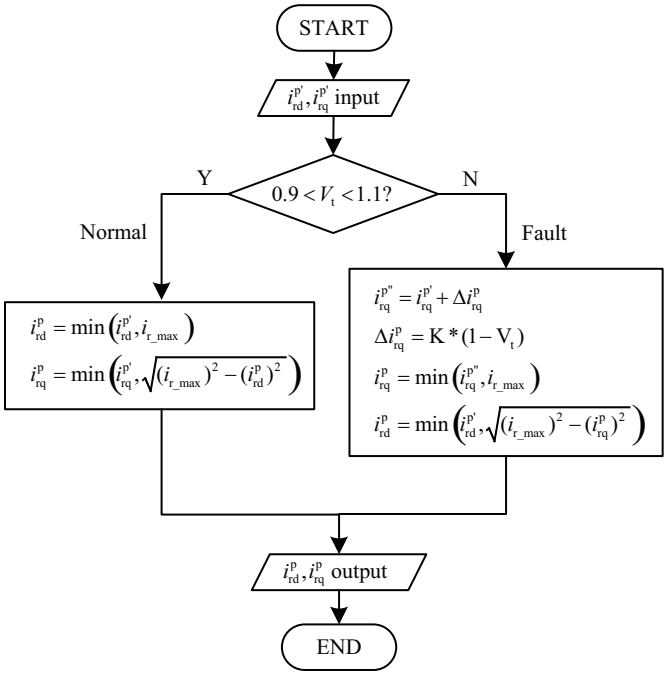

Fig. 11. Workflow of the normal/fault current control logic.

of the limited current capacity. As a result, the eventual d-axis rotor current is only limited by the current capacity of the converter.

$$i_{\mathrm{rd}}^{\mathrm{p}} = \min\left(i_{\mathrm{rd}}^{\mathrm{p}'}, i_{\mathrm{r\_max}}\right) \tag{21}$$

and the eventual q-axis rotor current will be limited by the remaining current capacity.

$$i_{\mathrm{rq}}^{\mathrm{p}} = \min\left(i_{\mathrm{rq}}^{\mathrm{p}'}, \sqrt{(i_{\mathrm{r\_max}})^2 - (i_{\mathrm{rd}}^{\mathrm{p}})^2}\right) \tag{22}$$

Under fault conditions, in addition to ensuring that the eventual apparent current of the rotor-side converter does not

exceed its current capacity, the logic also ensures that the resulting active and reactive currents injected into the grid satisfy the grid code requirements. Here, the grid code is the E.ON [23] whose requirements are illustrated in Fig. 12. It requires the WTG to preferentially inject extra reactive current proportional to the fault voltage deviation from the pre-fault voltage level. To meet the requirements, the logic adjusts the q-axis current commander $i_{\mathrm{rq}}^{\mathrm{p}'}$ as follows

$$i_{\mathrm{rq}}^{\mathrm{p}''} = i_{\mathrm{rq}}^{\mathrm{p}'} + \Delta i_{\mathrm{rq}} \tag{23}$$

$$\Delta i_{\mathrm{rq}} = \mathrm{K} * (1 - V_{\mathrm{t}}) \tag{24}$$

and endows the q-axis rotor current commander with the priority in the allocation of the current capacity. Hence, the q-axis will only be limited by the maximum current capacity of the converter.

$$i_{\mathrm{rq}}^{\mathrm{p}} = \min\left(i_{\mathrm{rq}}^{\mathrm{p}''}, i_{\mathrm{r\_max}}\right) \tag{25}$$

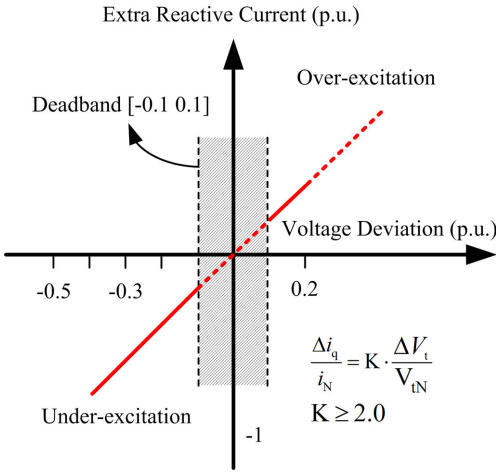

Fig. 12. Requirements of E.ON grid code on the WTG reactive current injection during fault.

Then, the d-axis rotor current will be limited by the remaining current capacity.

$$i_{\mathrm{rd}}^{\mathrm{p}} = \min\left(i_{\mathrm{rd}}^{\mathrm{p}'}, \sqrt{(i_{\mathrm{r\_max}})^2 - (i_{\mathrm{rq}}^{\mathrm{p}})^2}\right) \tag{26}$$

3) Stator Current Calculator

The d-axis and q-axis magnetizing currents $i_{\mathrm{rd}}^{\mathrm{p}}$ and $i_{\mathrm{rq}}^{\mathrm{p}}$ produced by the normal/fault current logic is sent to the stator current calculator to arrive at the resulting d-axis and q-axis currents injected into the grid through the stator interface. The calculation and its deduction are briefly introduced below.

The relationship between the terminal voltage of the WTG and its stator current and flux can be represented by

$$\boldsymbol{V_{\mathrm{t}}} = R_{\mathrm{s}}\boldsymbol{I_{\mathrm{s}}} + j\omega_{V_{\mathrm{t}}}\boldsymbol{\Psi_{\mathrm{s}}} + \frac{d\boldsymbol{\Psi_{\mathrm{s}}}}{dt} \tag{27}$$

Neglecting the stator transients [24],

$$\boldsymbol{V_{\mathrm{t}}} = R_{\mathrm{s}}\boldsymbol{I_{\mathrm{s}}} + j\omega_{V_{\mathrm{t}}}\boldsymbol{\Psi_{\mathrm{s}}} \tag{28}$$

Replacing $\omega_{V_{\mathrm{t}}}$ with ω_{pll} gives

$$\boldsymbol{V_{\mathrm{t}}} = R_{\mathrm{s}}\boldsymbol{I_{\mathrm{s}}} + j\omega_{\mathrm{pll}}\boldsymbol{\Psi_{\mathrm{s}}} \tag{29}$$

The stator flux is determined by the stator current and the rotor current.

$$\boldsymbol{\Psi_{\mathrm{s}}} = L_{\mathrm{s}}\boldsymbol{I_{\mathrm{s}}} + L_{\mathrm{m}}\boldsymbol{I}_r. \tag{30}$$

Thus, the relationship between the rotor excitation current generated by the rotor-side converter and the stator current is obtained.

$$\begin{aligned}\boldsymbol{I_{\mathrm{s}}} &= i_{\mathrm{sd}}^{\mathrm{p}} + j i_{\mathrm{sq}}^{\mathrm{p}} \\ &= \frac{R_{\mathrm{s}}V_{\mathrm{td}}^{\mathrm{p}} + \omega_{\mathrm{pll}}L_{\mathrm{s}}V_{\mathrm{tq}}^{\mathrm{p}} - \omega_{\mathrm{pll}}^2 L_{\mathrm{m}}L_{\mathrm{s}}i_{\mathrm{rd}}^{\mathrm{p}} + \omega_{\mathrm{pll}}L_{\mathrm{m}}R_{\mathrm{s}}i_{\mathrm{rq}}^{\mathrm{p}}}{R_{\mathrm{s}}^2 + \omega_{\mathrm{pll}}^2 L_{\mathrm{s}}^2} \\ &\quad + j\frac{R_{\mathrm{s}}V_{\mathrm{tq}}^{\mathrm{p}} - \omega_{\mathrm{pll}}L_{\mathrm{s}}V_{\mathrm{td}}^{\mathrm{p}} - \omega_{\mathrm{pll}}L_{\mathrm{m}}R_{\mathrm{s}}i_{\mathrm{rd}}^{\mathrm{p}} - \omega_{\mathrm{pll}}^2 L_{\mathrm{m}}L_{\mathrm{s}}i_{\mathrm{rq}}^{\mathrm{p}}}{R_{\mathrm{s}}^2 + \omega_{\mathrm{pll}}^2 L_{\mathrm{s}}^2}\end{aligned} \tag{31}$$

4) dq → abc: Transformation of the Coordinate System

The d-axis and q-axis currents from the stator current calculator will be added to the d-axis and q-axis currents injected into the grid through the grid-side converter to form the total d-axis and q-axis currents of the WTG. The transformation of the coordinate system transforms the d-axis and q-axis currents represented in the WTG rotating dq coordinate system into the three phase currents represented in the external grid static abc coordinate system.

$$\begin{bmatrix} i_{\mathrm{a}} \\ i_{\mathrm{b}} \\ i_{\mathrm{c}} \end{bmatrix} = \begin{bmatrix} \cos\theta_{\mathrm{pll}} & -\sin\theta_{\mathrm{pll}} \\ \cos(\theta_{\mathrm{pll}} - \frac{2\pi}{3}) & -\sin(\theta_{\mathrm{pll}} - \frac{2\pi}{3}) \\ \cos(\theta_{\mathrm{pll}} + \frac{2\pi}{3}) & -\sin(\theta_{\mathrm{pll}} + \frac{2\pi}{3}) \end{bmatrix} \begin{bmatrix} i_{\mathrm{d}}^{\mathrm{p}} \\ i_{\mathrm{q}}^{\mathrm{p}} \end{bmatrix} \tag{32}$$

where θ_{pll} is the output phase of the PLL.

5) PLL: Model of the Impacts of the PLL on the Transient Electromechanical Response of the WTG

The impacts of the PLL on the transient electromechanical response of the DFIG-based WTG, which has been theoretically analyzed in Section II, is modeled by incorporating the PLL in the proposed WTG electromechanical model.

Here, the PLL sub-model is similar to the one in the SIMULINK full-order DFIG-based WTG model. Fig. 13 illustrates the PLL structure. The three-phase terminal voltages are first transformed from the static abc coordinate system to the static $\alpha\beta$ coordinate system. The α-axis and β-axis components of the terminal voltage are used to calculate the magnitude of the terminal voltage before they are further transformed to the rotational dq coordinate system of the PLL. The resulting q-axis component of the terminal voltage is then taken as the monotonic phase error, and is sent to a classic PI controller to produce the deviated rotating speed $\Delta\omega$. Then the is added to the nominal rotating speed ω_0 to get the actual rotating speed of the PLL rotational dq coordinate system, ω. The output phase of the PLL θ_{pll} is obtained by integrating the ω.

Table I shows the default parameter settings of the PLL in the SIMULINK full-order model, which is also taken in the proposed model.

The bandwidth of the PLL is about 13 Hz. The calculation of the bandwidth is briefly introduced below. The closed loop

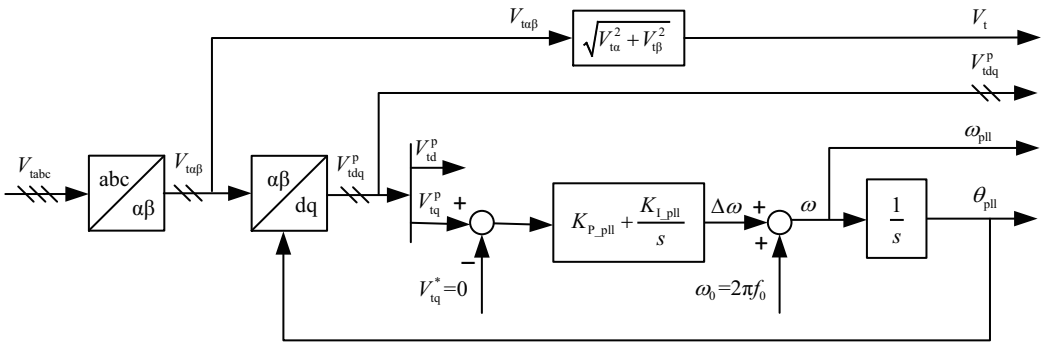

Fig. 13. Structure of the PLL in the SIMULINK full-order DFIG-based WTG model.

TABLE I
DEFAULT PARAMETER SETTINGS OF THE PLL

Parameter	Setting	Parameter	Setting
K_{P_pll}	60	K_{I_pll}	1,400

transfer function of the linearized PLL small-signal model is

$$H(s)=\frac{\theta_{pll}}{\theta_{V_t}}=\frac{K_{P\_pll}\cdot s+K_{I\_pll}}{s^2+K_{P\_pll}\cdot s+K_{I\_pll}} \tag{33}$$

The Bode plot of the PLL is obtained based on the transfer function and is shown in Fig. 14. The bandwidth of the PLL is the frequency when the magnitude Bode plot first decreases below the −3 dB, and as can be found from plot, the corresponding frequency is about 13 Hz.

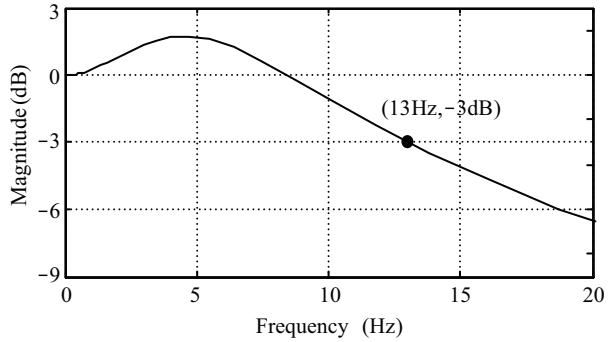

Fig. 14. Magnitude Bode diagram of the PLL.

B. Model Verification

The proposed reduced-order DFIG-based WTG model is verified by comparing to the SIMULINK full-order DFIG-based WTG model. The main differences in these models, as discussed in Section III-A, are that the proposed model simplifies the fast transients such as the current control loops and the electromagnetic transients in the DFIG machine. The PLL and the mechanical model of the proposed model are the same as the corresponding parts of the SIMULINK full-order model.

Fig. 15 shows the power system for verification and other purposes in this paper. A wind farm and a synchronous generator export power to the external grid through two transmission lines. The wind farm is modeled as an aggregated DFIG-based WTG, and the external grid is modeled by a synchronous generator and a load. A balanced 3-phase fault is applied to one of the transmission lines and the fault lasts for 500 ms.

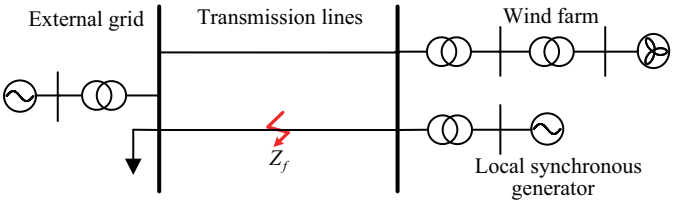

Fig. 15. Structure of the test power system.

Fig. 16 shows the simulation results. As the Fig. 16(a) and (b) illustrate, the overall power response of the proposed electromechanical reduced-order model matches well with that of the SIMULINK full-order model in the eletromechanical time scale, despite a small deviation of the active power over a

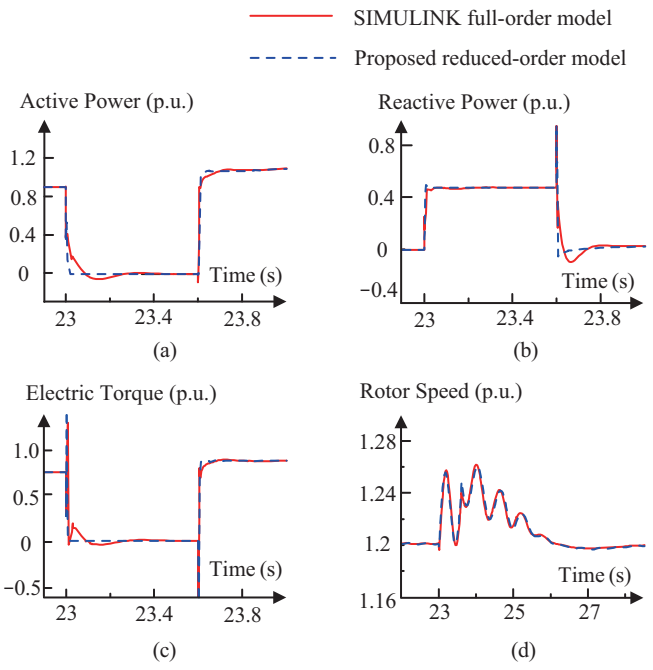

Fig. 16. WTG responses when the WTG model is the SIMULINK full-order model and the proposed reduced-order model. (a) Active power into the grid. (b) Reactive power into the grid. (c) Electric torque on the rotor of the DFIG generator. (d) Rotor speed of the DFIG generator.

short period after the fault occurrence and a small deviation of the reactive power over a short period after the fault clearance. Moreover, the dynamics of the inner variables of the WTG are also shown in Fig. 16(c)–(d). As can be found in the figures, the dynamics of the inner variables of the two models also match well in the electromechanical time scale. The results preliminarily verify the proposed model.

C. Model Analysis

1) Impact of Neglecting the PLL Sub-model on the Electromechanical Response of the Proposed WTG Model

The practice of the existing DFIG-based WTG electromechanical model that neglects the PLL as described in Section II-C is studied here using the proposed WTG electromechanical model. The absence of the PLL is modeled in the proposed model by removing the PLL sub-model and changing the sub-model of the coordinate system transformation from (2) to (14).

A same fault sequence as aforementioned is applied, and Fig. 17 demonstrates the simulation results when the PLL is incorporated or neglected in the proposed model. As the Fig. 17(a)–(b) present, the absence of the PLL causes a significant deviation in both the active and reactive power responses of the WTG, and the duration of the deviation is in the electromechanical time scale. Moreover, not including the PLL also leads to considerable deviations in the dynamics of the WTG inner variables, shown in Fig. 17(c)–(d). As the proposed model incorporating the PLL has been verified in Section III-B, the deviations can be interpreted as the deviation from the true responses. Therefore, it can be concluded that the PLL should not be overlooked to avoid possible significantly deviated responses as shown here.

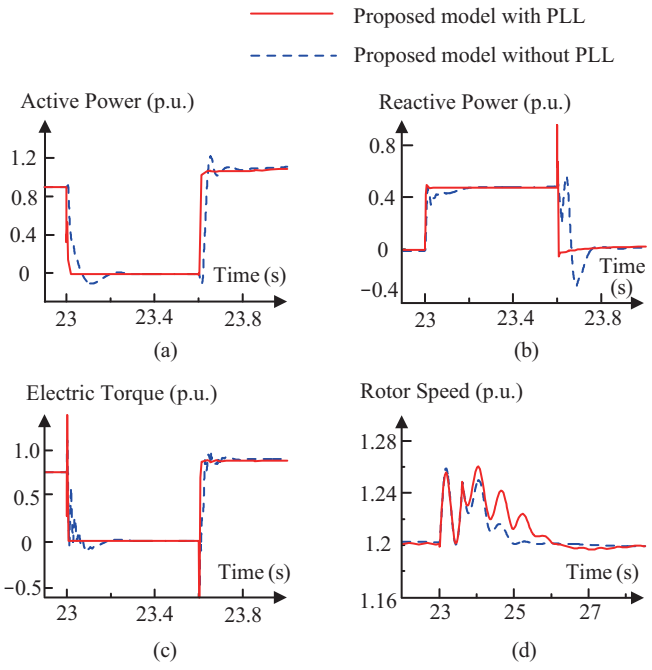

Fig. 17. Responses of the proposed reduced-order model when the PLL is incorporated or neglected. (a) Active power into the grid. (b) Reactive power into the grid. (c) Electric torque on the rotor of the DFIG generator. (d) Rotor speed of the DFIG generator.

2) Impacts of the Parameter Setting of the PLL Sub-model on the Electromechanical Response of the Proposed WTG Model

A modified parameter settings of the PLL sub-model of the proposed DFIG-based WTG model is designed and compared to the default parameter settings. The fault sequence aforementioned is applied. Fig. 18 demonstrates the simulation results. As can be found from the figure, the modified parameter setting of the PLL sub-model has significantly changed the output power and inner variable responses of the proposed WTG model. The WTG's active power response during fault-on period and its reactive power response after fault clearance, shown in Figs. 18(a) and Fig. 18(b) respectively, deviate significantly from those with the default PLL parameter setting. The dynamics of the WTG inner variables such as the rotating speed shown in Fig. 18(d) also deviate considerably.

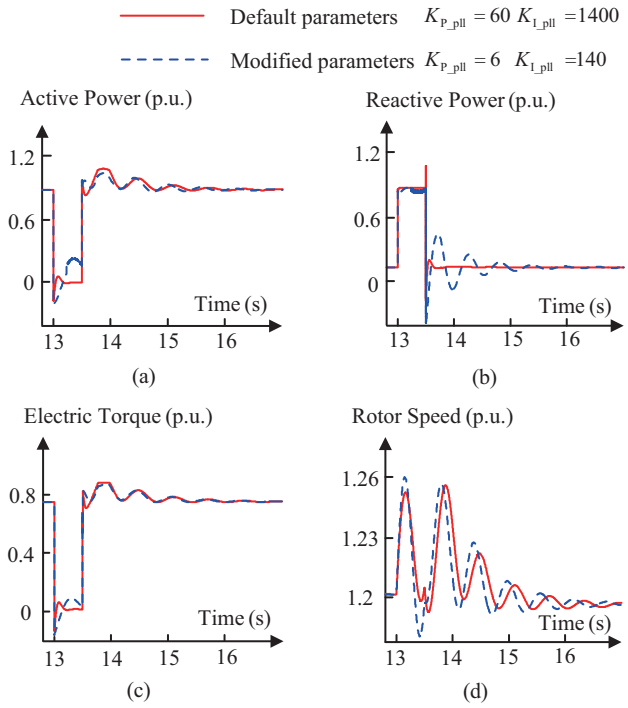

Fig. 18. Responses of the proposed reduced-order model when the parameters of the PLL sub-model remain in default or are modified. (a) Active power into the grid. (b) Reactive power into the grid. (c) Electric torque on the rotor of the DFIG generator. (d) Rotor speed of the DFIG generator.

A second fault that causes a higher fault voltage at the WTG terminal is also applied and cleared in a similar way. Fig. 19 exhibits the simulation results. Compared to Fig. 18, the deviation of the active power during the fault-on period has decreased significantly, but the deviation after the fault clearance has increased considerably, as shown in Fig. 19(a). Moreover, in addition to a significant deviation in the reactive power after the fault clearance, a large deviation during fault-on period can also be found in Fig. 19(b). The deviations in the WTG inner variables also increase significantly, which can be found in Fig. 19(c)–(d).

The considerable deviations shown in Fig. 18 and Fig. 19 demonstrate that the parameter setting of the PLL sub-model in

the proposed electromechanical model has significant impact on the electromechanical response of the whole model.

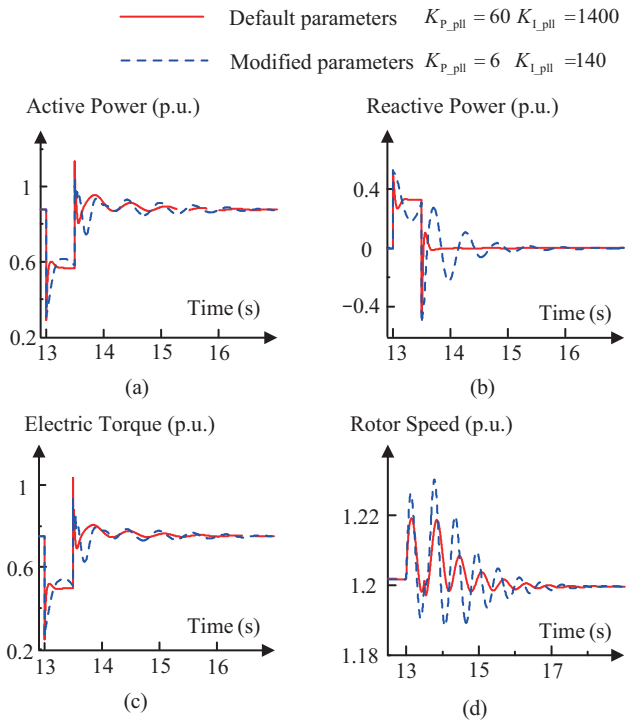

Fig. 19. Responses of the proposed reduced-order model when the parameters of the PLL sub-model remain in default or are modified. (a) Active power into the grid. (b) Reactive power into the grid. (c) Electric torque on the rotor of the DFIG generator. (d) Rotor speed of the DFIG generator.

IV. Conclusion

PLL impacts on the transient electromechanical responses of the DFIG-based WTG are studied in this paper via theoretical and time-domain simulation analysis. Theoretical analysis establishes the relationships between the WTG active and reactive current commanders, the actual WTG active and reactive currents injected into the grid, and the PLL dynamics, under normal and fault conditions when the PLL is incorporated or neglected. The relationships suggest that the PLL could significantly affect the response of the WTG. The theoretical analysis also discusses the bandwidth of the PLL and suggests that the impacts of the PLL on the WTG responses are in or near the electromechanical time scale.

In the time-domain simulation analysis, a reduced-order electromechanical DFIG-based WTG model is proposed and preliminarily verified by comparing to the SIMULINK full-order DFIG-based WTG model. The impact of neglecting the PLL when establishing the WTG electromechanical model is then studied based on the proposed electromechanical model. The simulation results show that neglecting the PLL could cause the response of the eletromechanical model to deviate considerably from the true response. Additionally, the impact of the parameter setting of the PLL sub-model in the proposed WTG model is studied. The simulation results suggest that the parameter setting of the PLL sub-model has a heavy influence on the response of the whole WTG model.

Therefore, this paper suggests that the impact of the PLL should not be neglected, but should be considered carefully when establishing the WTG electromechanical model. Note that the PLLs employed by the field WTGs vary in the structure and the parameter setting [20], [22], [25], and this paper only studies one of them. More studies that consider different structures of the PLL are expected. In addition, the modeling of the impacts of the PLL in this paper is to keep the PLL in the WTG electromechanical model without any simplifications, which increases the order and the complexity of the model and is not generic either. A simple, low-order and generic model for the impact of the PLL on the WTG electromechanical response is expected.

References

[1] "2014 IEA wind annual report," IEA, 2015.
[2] T. Petru and T. Thiringer, "Modeling of wind turbines for power system studies," *IEEE Transactions on Power Systems*, vol. 17, no. 4, pp. 1132–1139, Nov. 2002.
[3] M. Bongiorno and T. Thiringer, "A generic DFIG model for voltage dip ride-through analysis," *IEEE Transactions on Energy Conversion*, vol. 28, no. 1, pp. 76–85, Mar. 2013.
[4] S. Chandrasekar and R. Gokaraju, "Dynamic phasor modeling of type 3 DFIG wind generators (including SSCI phenomenon) for short-circuit calculations," *IEEE Transactions on Power Delivery*, vol. 30, no. 2, pp. 887–897, Apr. 2015.
[5] J. B. Hu, Y. H. Huang, D. Wang, H. Yuan, and X. M. Yuan, "Modeling of grid-connected DFIG-based wind turbines for DC-link voltage stability analysis," *IEEE Transactions on Sustainable Energy*, vol. 6, no. 4, pp. 1325–1336, Oct. 2015.
[6] J. Y. Ruan, Z. X. Lu, Y. Qiao, Y. Min, G. H. Shao, X. W. Xu, and K. Y. Hou, "Transient stability of wind turbine adopting a generic model of DFIG and singularity-induced instability of generators/units with power–electronic interface," *IEEE Transactions on Energy Conversion*, vol. 30, no. 3, pp. 1069–1080, Sep. 2015.
[7] K. M. Alawasa, Y. A. R. I. Mohamed and W. Xu, "Modeling, analysis, suppression of the impact of full-scale wind-power converters on subsynchronous damping," *IEEE Systems Journal*, vol. 7, no. 4, pp. 700–712, Dec. 2013.
[8] V. Akhmatov, H. Knudsen, A. H. Nielsen, J. K. Pedersen, and N. K. Poulsen, "Modeling and transient stability of large wind farms," *International Journal of Electrical Power & Energy Systems*, vol. 25, no. 2, pp. 123–144, Feb. 2003.
[9] P. Ledesma and J. Usaola, "Doubly fed induction generator model for transient stability analysis," *IEEE Transactions on Energy Conversion*, vol. 20, no. 2, pp. 388–397, Jun. 2005.
[10] J. Kretschmann, H. Wrede, S. Mueller-Engelhardt, and I. Erlich, "Enhanced reduced order model of wind turbines with DFIG for power system stability studies," in *Proceedings of PECon*, Kuala Lumpur, Malaysia, Nov. 28–29, 2006, pp. 303–311.
[11] Y. Lei, A. Mullane, G. Lightbody, and R. Yacamini, "Modeling of the wind turbine with a doubly fed induction generator for grid integration studies," *IEEE Transactions on Energy Conversion*, vol. 21, no. 1, pp. 257–264, Mar. 2006.
[12] I. Erlich, J. Kretschmann, J. Fortmann, S. Mueller-Engelhardt, and H. Wrede, "Modeling of wind turbines based on doubly-fed induction generators for power system stability studies," *IEEE Transactions on Power Systems*, vol. 22, no. 3, pp. 909–919, Aug. 2007.
[13] K. Clark, N. W. Miller, and J. J. Sanchez-Casca, "Modeling of GE wind turbine-generators for grid studies," GE Energy, Apr. 2010.
[14] Y. J. Wang, J. B. Hu, D. L. Zhang, C. Ye, and Q. Li, "DFIG WT electromechanical transient behaviour influenced By PLL: modelling and analysis," in 4^{th} *International Conference on Renewable Power Generation*, Beijing, 2015, pp. 1–5.
[15] P. Pourbeik. (2011, Dec.). Generic models and model validation for wind and solar PV generation: Technical update. EPRI. Palo Alto, California. [Online]. Available: http://www.epri.com/abstracts/pages/productabstract.aspx?ProductID=000000000001021763&Mode=download

[16] P. Pourbeik. (2012, Jul.). Proposed changes to the WECC WT4 generic model for type 4 wind turbine generators. EPRI. Palo Alto, California. [Online]. Available: https://www.wecc.biz/Reliability/Report_on_WT4_Model_Description_PP012313.pdf
[17] P. Pourbeik. (2013, Sep.). Proposed changes to the WECC WT3 generic model for type 3 wind turbine generators. EPRI. Palo Alto, California. [Online]. Available: https://www.wecc.biz/Reliability/WECC-Type-3-Wind-Turbine-Generator-Model-Phase-II-012314.pdf
[18] *Wind Turbines - Part 27-1: Electrical Simulation Models*, IEC Standard IEC 61400-27-1:2015.
[19] X. M. Yuan, Z. H. Tan, R. W. Delmerico, H. Q. Weng, and R. A. Seymour, "Phase-locked-loop circuit," U.S. Patent 7 928 780, Sep. 29, 2009.
[20] North American Electric Reliability Corporation. (2010, May). Special report - Standard models for variable generation. North American Electric Reliability Corporation. [Online]. Available: http://www.uwig.org/Standard_Models_for_Variable_Generation.pdf
[21] A. V. Timbus, M. Liserre, R. Teodorescu, and F. Blaabjerg, "Synchronization methods for three phase distributed power generation systems. An overview and evaluation," in *Proceedings of IEEE PESC, 2005*, pp. 2474–2481.
[22] L. Hadjidemetriou, E. Kyriakides, and F. Blaabjerg, "A new hybrid PLL for interconnecting renewable energy systems to the grid," *IEEE Transactions on Industry Applications*, vol. 49, no. 6, pp. 2709–2719, Nov. 2013.
[23] "Grid code—high and extra high voltage," E.ON Netz GmbH, Bayreuth, Germany, Apr. 2006.
[24] P. Ledesma and J. Usaola, "Effect of neglecting stator transients in doubly fed induction generator models," *IEEE Transactions on Energy Conversion*, vol. 19, no. 2, pp. 459–461, Jun. 2004.
[25] A. Nagliero, R. A. Mastromauro, M. Liserre, and A. Dell'Aquila, "Synchronization techniques for grid connected wind turbines," in *Proceedings of 35th IEEE IECON*, 2009, pp. 4606–4613.

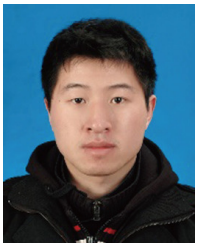

Dongliang Zhang (S'13) was born in Zibo, China, in 1989. He received the B.Eng. degree in School of Electrical Engineering at Shandong University (SDU), Jinan, China, in July 2011. He is currently pursuing the Ph.D. degree in State Key Laboratory of Advanced Electromagnetic Engineering and Technology, and School of Electrical and Electronic Engineering, Huazhong University of Science and Technology, Wuhan, China. His current research interest includes the impacts of the integration of wind power on the stability of the power system and methods to increase the stability support from the wind power.

Yajing Wang was born in Hubei, China, in 1991. She received the B.Sc. degree from School of Hydropower & Information Engineering, Huazhong University of Science and Technology, Wuhan, China, in 2012 and the M.Sc. degree in State Key Laboratory of Advanced Electromagnetic Engineering and Technology, from School of Electrical and Electronic Engineering, Huazhong University of Science and Technology, Wuhan, China, in 2015. She currently works in Ningbo Electric Power Design Institute Co., Ltd. Her research interests include power systems, renewable energy generation.

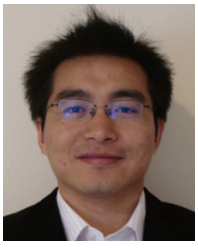

Jiabing Hu (S'05–M'10–SM'12) received the B.Eng. and Ph.D. degrees in College of Electrical Engineering, Zhejiang University, Hangzhou, China, in July 2004 and September 2009, respectively. From 2007 to 2008, he was funded by Chinese Scholarship Council (CSC) as a visiting scholar with the Department of Electronic and Electrical Engineering, University of Strathclyde, Glasgow, U.K. From April 2010 to August 2011, he was a Post-Doctoral Research Associate with Sheffield Siemens Wind Power (S2WP) Research Center and the Department of Electronic and Electrical Engineering, University of Sheffield, Sheffield, U.K. Since September 2011, he has been a Professor with State Key Laboratory of Advanced Electromagnetic Engineering and Technology, and School of Electrical and Electronic Engineering, Huazhong University of Science and Technology, Wuhan, China. His current research interests include grid-integration of large-scale renewables, modular multilevel converter (MMC) for HVDC applications, and transient analysis and control of semiconducting power systems.

He is the author/coauthor of more than 70 peer-reviewed technical papers and one monograph "Control and Operation of Grid-Connected Doubly-Fed Induction Generators," and holds more than 20 issued/pending patents. Dr. Hu received the 2014 Top Ten Excellent Young Staff Award from Huazhong University of Science and Technology, and is currently supported by the National Natural Science of China for Excellent Young Scholars and the Program for New Century Excellent Talents in University from Chinese Ministry of Education. He serves as Domestic Member of the Editorial Board for Frontiers of Information Technology and Electronic Engineering (FITEE) formerly known as Journal of Zhejiang University-SCIENCE C.

Shicong Ma (M'12) was born in Wudi, China, in 1980. He was awarded the Ph.D. degree by Shandong University, China, in 2008. His employment experiences include Kehui Power Automation Co. Ltd., China, Alstom Grid, U.K. Now he is employed by CEPRI. His research interests include power system stability and security, data mining in power system, protection and fault location.

Qing He was born in 1980. He was awarded Ph.D. by China Electric Power Research Institute. He is currently a Senior Engineer in the power systems department of China Electric Power Research Institute. His research interests include power system complexity, power system operation and control. He participated in security and stability analysis of UHV AC engineering and UHV DC engineering.

Qiang Guo was born in 1972. He is currently a professorate Senior Engineer in the power systems department of China Electric Power Research Institute. His research interests include power system planning, power system analysis, and FACTS. He has long been engaged in UHV power grid planning. In China's 2030 and 2050 ultra-high voltage planning, he has made an important contribution.